# Synthesis of Multi-Walled Carbon Nanotubes by Fluidized-Bed Chemical Vapor Deposition over Co/Al2O3

S. Pooperasupong, Brigitte Caussat, Philippe Serp, S. Damronglerd

# Synthesis of Multi-Walled Carbon Nanotubes by Fluidized-Bed Chemical Vapor Deposition over $Co/Al_2O_3$

Sompoch Pooperasupong[1], Brigitte Caussat[2], Philippe Serp[3] and Somsak Damronglerd[1]

[1] *Department of Chemical Technology, Faculty of Science, Chulalongkorn University, Phayathai Road, Pathumwan, Bangkok 10330, Thailand*

[2] *Laboratoire de Génie Chimique UMR CNRS 5503, ENSIACET/INPT, Université de Toulouse, 4 allée Emile Monso, BP 44362, 31030 Toulouse Cedex 4, France*

[3] *Laboratoire de Chimie de Coordination UPR CNRS 8241, Composante ENSIACET, Université de Toulouse, 4 allée Emile Monso, BP 44362, 31030 Toulouse Cedex 4, France*

**Keywords:** Carbon Nanotubes, Chemical Vapor Deposition, Fluidization, Cobalt Catalyst, Ethylene

**Synthesis of multi-walled carbon nanotubes (MWCNTs) was accomplished by catalytic chemical vapor deposition of ethylene over $Co/Al_2O_3$ in a fluidized-bed. The reaction temperature and ethylene concentration, as the molar percentage (mol%), were both found to be crucial factors determining the solid carbon conversion level and selectivity of MWCNT formation, but had no significant effect on the size distribution of the obtained MWCNTs. Amorphous carbon and carbon nanofibers (CNFs) were the main products obtained at a reaction temperature of 550°C. Amorphous carbon was also formed when using ethylene at a high concentration (62.5 mol%), which possibly deactivated the catalyst. Increasing the reaction temperature from 550 to 650°C resulted in better graphitized MWCNTs. The average diameters of the synthesized MWCNTs were in the range of 7–8 nm independent of the reaction temperature or ethylene concentration. The selectivity of alkane production decreased considerably at reaction temperatures above 675°C, resulting in a higher productivity of MWCNTs. The activation energy for MWCNT formation was found to be 65.3 kJ/mol, which matched well with that previously reported for carbon diffusion in liquid cobalt.**

## Introduction

Over the last two decades, since their first discovery as a by-product on the cathode of an arc-discharge reactor during fullerene production (Iijima, 1991), carbon nanotubes (CNTs) have been anticipated to be "materials for the future". This is due to their outstanding mechanical, electrical, thermal and magnetic properties that make these nanostructure materials suitable for various applications (Serp *et al.*, 2003; Terrones, 2003; Paradise and Goswami, 2007). Today, many industrial groups are focusing on ways of applying CNTs to their products, as seen from the continual increase in the number of application-related articles. To meet the current and future needs of these different fields or industries, the bulk production of CNTs is still a challenge facing researchers (Philippe *et al.*, 2007; Zhang *et al.*, 2011).

Among the different techniques that have been developed to produce CNTs, fluidized-bed catalytic chemical vapor deposition (FB-CCVD) is considered to be the most promising technology for the industrial scale production of CNTs due to its simplicity, flexibility, considerably low operating cost and high productivity level (Venegoni *et al.*, 2002; Wang *et al.*, 2002; Corrias *et al.*, 2005; McCaldin *et al.*, 2006; Vahlas *et al.*, 2006; Escobar *et al.*, 2007; Morançais *et al.*, 2007; Philippe *et al.*, 2007, 2009; See and Harris, 2007; Paradise and Goswami, 2007; Zhang *et al.*, 2011). This process has already been developed and established worldwide for the production of single-walled CNT and multi-walled CNTs (MWCNTs) in many countries, such as Belgium (Nanocyl), France (Arkema), Germany (Bayer Material Science), Japan (Showa Denko) and the U.S.A. (SouthWest NanoTechnologies). Unfortunately, details concerning such scale up processes are very limited in the open literature.

Besides improvements in reactor technology, finding new catalysts for growing CNTs has also received scientific interest. The use of transition metals, such as iron, nickel, cobalt and molybdenum, and bimetallic alloys have both been widely reported for the large-scale synthesis of CNTs (Danafar *et al.*, 2009; Kumar and Ando, 2010). Recently, alternatives to these transition metal catalysts have been proposed, such as $SiO_2$ (Huang *et al.*, 2009; Xu *et al.*, 2012b), $Al_2O_3$, $TiO_2$ (Huang *et al.*, 2009) and even stainless steel (Baddour *et al.*, 2009; Camilli *et al.*, 2011). However, most of them have only been evaluated at a laboratory scale and still need further development.

Ethylene, used as a reactant in the general chemical industry, is one of the most interesting carbon sources as a precursor for MWCNT synthesis because its moderate thermal stability allows it to be readily decomposed at a controllable rate at a low temperature (Corrias *et al.*, 2005; Morançais *et al.*, 2007; Philippe *et al.*, 2009).

DOI: 10.1252/jcej.13we068

Correspondence concerning this article should be addressed to S. Damronglerd (E-mail address: damronglerd_s@yahoo.co.th).

In order to efficiently produce MWCNTs on a large scale, it is important to understand the effect of the process parameters on the reaction kinetics and formation efficiency, as well as on the physical properties of the obtained MWCNTs, so as to be able to optimize the design and execution of the industrial process for their production. In this article, therefore, the production of MWCNTs over Co/$Al_2O_3$ via a FB-CCVD process using ethylene as the precursor was evaluated. The influences of the process parameters on the productivity and selectivity of MWCNTs, as well as their characteristics, is presented. Moreover, a kinetic study is also reported in order to illustrate the apparent initial kinetic parameters for the growth of MWCNTs.

## 1. Experimental

### 1.1 Materials and chemicals

The cobalt impregnated (3.3% by weight) gamma-alumina (Co/$Al_2O_3$) catalyst used in this research was provided by Laboratoire de Chimie de Coordination, and was calcined at 450°C for 6 h in air at a flow rate of 400 standard $cm^3$/min (sccm). Electronics grade ethylene, hydrogen ($H_2$) and nitrogen ($N_2$) (Air Liquide) were used as the fluidizing gas.

### 1.2 Experimental set-up and procedure

The FB-CCVD reactor used in this study (**Figure 1**) was made of 304 L stainless steel and contained a cylindrical zone of 5 cm inner diameter, 1 m height and an expansion zone of 10 cm inner diameter, which allows particles to drop back into the bed. The gas distributor was comprised of a double layered stainless steel grid with 40 μm holes. Corrugated stainless steel packing media was added (15 cm height) below the gas distributor to ensure excellent uniformity of the fluidizing gas temperature. The bed temperature was controlled by a temperature control system comprised of electric furnaces, proportional-integral-derivative temperature controllers and two thermocouples located at the central axis of the reactor at 5 and 40 cm above the distributor. A pressure sensor was also installed in order to measure the pressure drop across the bed and the total pressure in the reactor. Fine particles (soot) that were generated as by-products were entrapped by a bag filter.

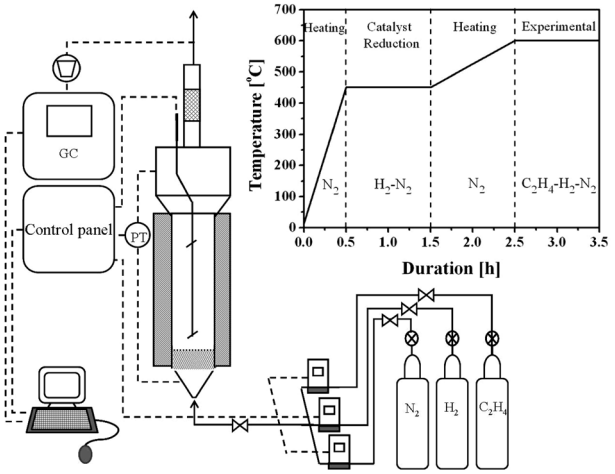


**Fig. 1** Schematic diagram of the experimental setup and (insert graph) the reaction procedure

Details of the general procedure are as follows. Initially, the designated amount of calcined Co/$Al_2O_3$ catalyst powder (20 or 60 g) was loaded into the reactor. The bed was then concurrently fluidized and heated up to 450°C at a rate of 15°C/min under a 400 : 400 sccm $H_2$ : $N_2$ flow, and then maintained at 450°C for 1 h to reduce the cobalt(II, III) oxide ($Co_3O_4$). The temperature was then raised under a flow of pure $N_2$ until the desired reaction temperature was attained. As soon as the temperature was steady, the flow rate of $N_2$ was decreased, while ethylene and $H_2$ were introduced simultaneously into the reactor at the pre-calculated flow rate.

For all experiments, the total volumetric flow rate of the fluidizing gas was 800 sccm, corresponding to a superficial gas velocity ($U$) at 700°C of about 8 $U_{mf}$. After completion of the reaction, the bed was cooled down to ambient temperature under a flow of $N_2$ and the composite (Co/$Al_2O_3$ catalyst powders and carbonaceous deposit) was removed for further characterization. A schematic diagram of the experimental setup and procedure is given in Figure 1.

Initially, the effect of temperature on the synthesis of MWCNTs was evaluated from 550–700°C with a fixed 60 min reaction time and 20 g of Co/$Al_2O_3$ catalyst. The flow rate of ethylene, $H_2$ and $N_2$ were fixed at 400, 200 and 200 sccm, respectively. The mass of introduced carbon was approximately 0.4 g/min.

Then, the influence of the ethylene concentration, as molar percentage (mol%), was evaluated over the range of 37.5–62.5 mol% by changing its flow rate. The flow of ethylene and $N_2$ were varied concurrently from 300 : 300 sccm to 500 : 100 sccm; whereas, the flow of $H_2$ was kept constant at 200 sccm. Each reaction was performed at 600°C for 60 min using 20 g of Co/$Al_2O_3$ catalyst.

Finally, the kinetics of the synthesis of MWCNTs was evaluated over the temperature range of 600–700°C with a fixed amount (60 g) of Co/$Al_2O_3$ catalyst and with all the other parameters being the same as in the first part (we explain later (Section 2.5) why the amount of catalyst was changed). The composition of the effluent gas was analyzed by online gas chromatography (GC) every 10 min.

In order to evaluate the process efficiency, the solid carbon conversion [%], defined as the ratio of the mass of carbonaceous deposits to the mass of introduced carbon, the selectivity [%], defined as the ratio of the mass of MWCNTs to the mass of carbonaceous deposits, and the productivity '$X_i$' [$g_C/g_{cat}$], defined as the ratio of the mass of carbon in the form of product $i$ to the mass of catalyst, were analyzed in each case.

### 1.3 Characterization of the Co/$Al_2O_3$ catalyst and products

The percentage of carbonaceous deposits, in the form of amorphous carbon, carbon nanofibers (CNFs) and

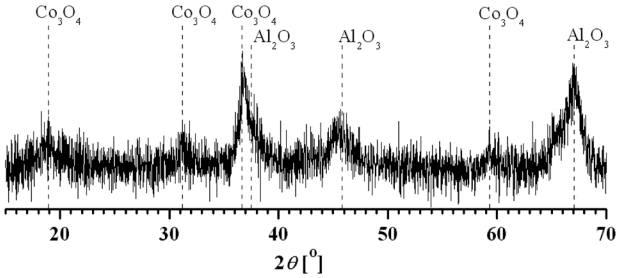


**Fig. 2** XRD pattern of the freshly prepared $Co/Al_2O_3$ catalyst after being calcined at 450°C; the pattern shown is representative of those seen from two independent samples

MWCNTs, was analyzed by thermo-gravimetric/derivative thermo-gravimetric (TG/DTG) analysis using a Mettler Toledo 851e instrument. The TG/DTG analysis was operated from 30–1000°C with a ramp rate of 10°C/min under a 50 mL/min flow of pure oxygen.

The crystalline structure of the catalyst and synthesized products were analyzed by X-ray powder diffractometry (XRD) using a Bruker D8 Advance XRD system employing Cu$K\alpha$ radiation ($\lambda = 1.5406$ Å) with an X-ray power of 40 kV and 40 mA. The $2\theta$ measurement was taken from 15–90° with a step of 0.0092° and a count time of 1 s/step.

The morphology of the formed products was examined by scanning electron microscopy (SEM) and transmission electron microscopy (TEM) on a LEO 435 and Philips CM-12, respectively. For the SEM analysis, the dried samples were mounted on a stub with C tape and examined using an accelerating voltage of 10 kV. For the TEM analysis, the samples dispersed in ethanol were applied onto a Cu grid and examined using an accelerating voltage of 120 kV.

## 2. Results and Discussion

### 2.1 Catalyst characterization

The XRD pattern of the crystalline phase of the calcined $Co/Al_2O_3$ catalyst (**Figure 2**) revealed diffraction angles that corresponded to two separate phases. The first was cobalt(II, III) oxide ($Co_3O_4$) with diffraction angles at $2\theta = 19.0°$ (1 1 1), 31.3° (2 2 0), 36.8° (3 1 1) and 59.4° (5 1 1), while the second phase was gamma-alumina ($\gamma$-$Al_2O_3$) with diffraction angles at $2\theta = 37.6°$ (3 1 1), 45.9° (4 0 0) and 67.0° (4 4 0).

Because the *in-situ* reduction of the $Co_3O_4$ catalyst was performed before the synthesis of MWCNTs, the real active phase for growing MWCNTs was not $Co_3O_4$, but $Co^0$. However, analysis of the crystallite size of $Co^0$ is difficult since it is highly reactive and readily oxidized when exposed to air even at an ambient temperature. Therefore, the crystallite size ($D$) of $Co^0$ was indirectly estimated from that of $Co_3O_4$ by converting the latter to the former according to their relative molar volumes (Schanke *et al.*, 1995), as shown in Eq. (1).

$$D_{Co^0} = 0.75 \times D_{Co_3O_4} \quad (1)$$

The mean crystallite size of $Co_3O_4$, calculated from line broadening at half the maximum intensity and the Bragg angle of the (3 1 1) diffraction peak using the Debye–Scherrer equation, was found to be 9.4±0.6 nm, and so the mean crystallite size of $Co^0$, as estimated by Eq. (1), was 7.1±0.5 nm. The SEM image and major characteristics of the fresh catalyst after being calcined at 450°C are shown in **Figure 3** and **Table 1**, respectively.

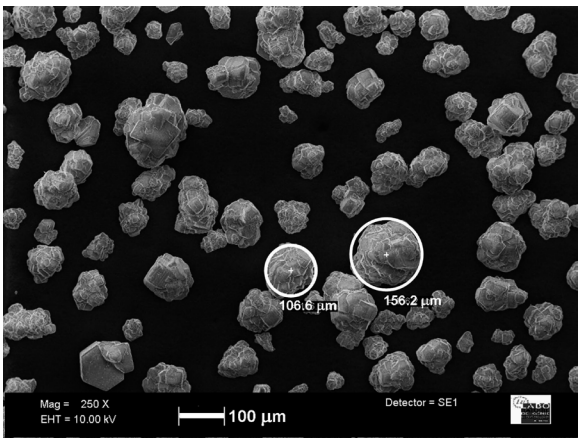


**Fig. 3** SEM image (250× magnification) of the freshly prepared $Co/Al_2O_3$ catalyst after being calcined at 450°C; image shown is representative of those seen from at least two such fields of view per sample and two independent samples; scale bar is 100 µm; circles show particles with a diameter of (left) 106.6 µm and (right) 156.2 µm

### 2.2 Effect of the process parameters on the synthesis of MWCNTs

The effect of the process parameters on the synthesis of MWCNTs was determined by comparing the solid carbon conversion level and the MWCNT selectivity. The bed weight gain was considered to be the mass of the carbonaceous deposits and was used for calculating the solid carbon conversion, while the MWCNT selectivity was evaluated by TG/DTG analysis.

2.2.1 Influence of the temperature The TG/DTG analysis of the products synthesized at different temperatures typically (but not for that at 550°C) showed two dominant steps (**Figure 4**). The first step corresponded to the weight loss of the amorphous carbon that readily burns at a low temperature, while the second step was the loss due to burning of the MWCNTs that occurs at a higher temperature.

However, the TG/DTG analysis of the product synthesized at 550°C (Figure 4(a)) did not reveal two clear deg-

**Table 1** Characteristics of the freshly prepared $Co/Al_2O_3$ catalyst after being calcined at 450°C

| $\rho_g$ [a] [g/cm³] | $\rho_b$ [b] [g/cm³] | $D_{Co}$ [0] [nm] | $D_{[4,3]}$ [c] [μm] | Surface area [d] [m²/g] | $U_{mf}$ [cm/s] | % Co [e] [wt%] |
|---|---|---|---|---|---|---|
| 3.31±0.03 | 1.01±0.001 | 7.1±0.5 | 81.0±0.6 | 158.2±4.5 | 0.31±0.03 | 3.30±0.05 |

Data are shown as the mean±1 S.D. and are derived from two independent samples. [a] Water pycnometry, [b] Hosokawa PT-E powder tester (ASTM D6393-99), [c] Laser-granulometry, [d] $N_2$ adsorption/desorption, [e] ICP-MS

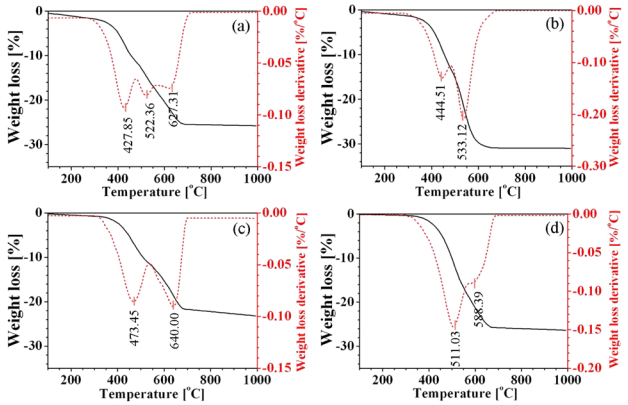


**Fig. 4** TG/DTG curves of the product synthesized at (a) 550°C, (b) 600°C, (c) 650°C and (d) 700°C; curves shown are representative of those seen from two independent samples

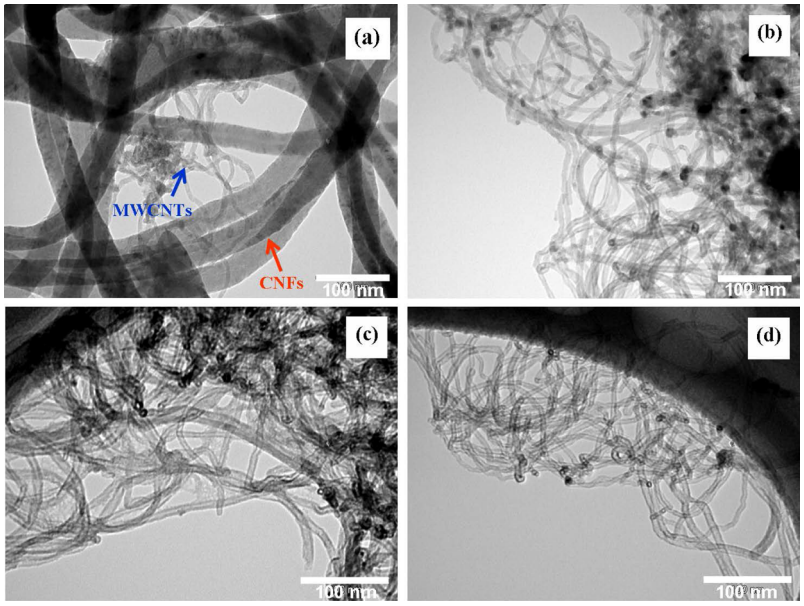


**Fig. 5** TEM images of the product synthesized at (a) 550°C, (b) 600°C, (c) 650°C and (d) 700°C; other reaction conditions were constant at 60 min with 20 g catalyst and an ethylene, $H_2$ and $N_2$ flow rate of 400, 200 and 200 sscm, respectively; images shown are representative of those seen from at least three such fields of view per sample and two independent samples; scale bars are 100 nm

radation steps in the thermal oxidation, presumably due to the presence of the additional product, CNFs, as seen in the TEM image (**Figure 5(a)**). The occurrence of these nanostructured materials as co-products could result in the low selectivity of MWCNTs.

It is noteworthy that the product synthesized at 600°C had a low thermal stability when considering its temperature at the maximum rate of weight loss (oxidation temperature, '$T_o$'), and the TEM images revealed that the product obtained at this temperature was mainly comprised of MWCNTs and not CNFs (**Figure 5(b)**). One conceivable explanation for this apparent discrepancy is that the MWCNTs synthesized at this temperature may be poorly graphitized. This assumption was supported by the evaluation of the crystallinity of the samples (Section 2.3).

The effect of temperature on the synthesis of MWCNTs is summarized in **Table 2**. Unsurprisingly, the solid carbon conversion level and MWCNT selectivity were quite low at 550°C, since this temperature is insufficient for both ethylene dissociation and MWCNT formation (Morançais *et*

*al.*, 2007; Philippe *et al.*, 2007, 2009). Raising the reaction temperature to 600°C led to a marked (2.29-fold) increase in the solid carbon conversion level, indicating that sufficient external energy was available for ethylene dissociation. Moreover, it also allowed the formation of MWCNTs (albeit with a defective structure), resulting in the increased (1.84-fold) MWCNT selectivity. Nevertheless, further increasing the reaction temperature above 600°C led to reduced levels of solid carbon conversion (1.49-fold) and MWCNT selectivity (1.22-fold).

The decreased level of MWCNT production with respect to temperatures above 600°C is possibly due to the rapid-decomposition of ethylene catalyzed by the metal catalyst to form a deposit of amorphous carbon, as previously reported elsewhere (Gulino *et al.*, 2005; Morançais *et al.*, 2007; Somanathan and Pandurangan, 2010).

2.2.2 Influence of the ethylene concentration [mol%]

The effect of the ethylene concentration (as mol%) on the solid carbon conversion level, MWCNT selectivity, and the thermal oxidation temperature of the obtained products are summarized in **Table 3**, with representative TG/DTG profiles shown in **Figure 6**. Increasing the ethylene concentration from 37.5 to 50.0 mol% markedly increased the solid carbon conversion level (2.9-fold) without any dramatic effect on the MWCNT selectivity (1.1-fold increase). This can be explained by the kinetic law governing the formation of MWCNTs, which has a positive order dependent on the ethylene concentration, as shown in Eq. (2).

$$dX/dt = (k)\left[C_2H_4\right]^a \quad (2)$$

Herein, $dX/dt$ is the MWCNT formation rate, $k$ is the rate constant, and $a$ is the kinetic order, respectively. Because the reaction was of a fixed duration (60 min), the low solid carbon conversion level obtained at a low ethylene concentration is somewhat logical.

In addition, we suppose that a change in fluidizing gas composition could also affect the fluidization quality of the bed. Since $N_2$ was used as a balancing gas, lowering the ethylene content, the fluidizing gas was more viscous. The increased gas viscosity allows the formation of large bubbles that then make the wall-effect dominant and reduce the gas–solid contact in this small reactor, resulting in the low solid carbon conversion level.

Moreover, we believe that the loss in fluidizability also

**Table 2** The carbon conversion efficiency, selectivity for MWCNT synthesis and thermal oxidation temperature ($T_o$) for MWCNT synthesis at different temperatures

| Temperature [°C] | Solid carbon conversion [%] | MWCNT selectivity [%] | $T_o$ [°C] |
|---|---|---|---|
| 550 | 27.9±1.1 | 26.3±1.2 | 524±1.9 |
| | | 29.3±3.7 | 626±1.6 |
| 600 | 65.1±1.2 | 56.1±3.5 | 532±1.9 |
| 650 | 42.5±0.6 | 47.1±1.3 | 639±2.1 |
| 700 | 41.9±1.5 | 40.6±2.2 | 589±1.1 |

Data are shown as the mean ±1 S.D. and are derived from two independent samples.

**Table 3** The carbon conversion efficiency, selectivity for MWCNT synthesis and thermal oxidation temperature ($T_o$) for the MWCNT synthesis at different ethylene concentrations [mol%]

| $C_2H_4$ [mol %] | Solid carbon conversion [%] | MWCNT selectivity [%] | $T_o$ [°C] |
|---|---|---|---|
| 37.5 | 24.5±2.3 | 52.5±6.8 | 550±2.0 |
| 50.0 | 65.1±1.2 | 56.1±3.5 | 532±1.9 |
| 62.5 | 21.5±1.2 | 28.4±1.5 | 575±2.2 |

Data are shown as the mean±1 S.D. and are derived from two independent samples.

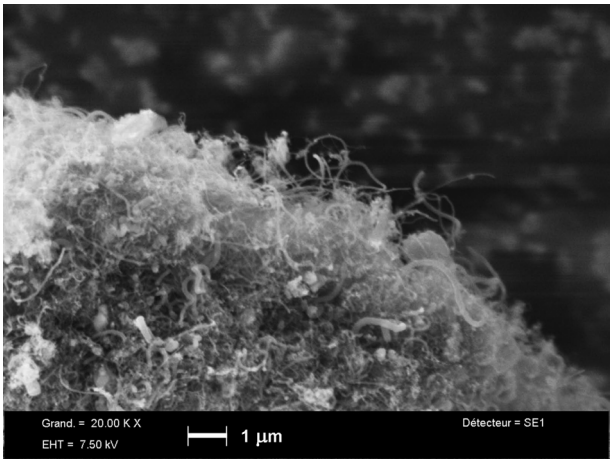


**Fig. 7** SEM image (20,000×magnification) of product synthesized with 62.5 mol% of ethylene; other reaction conditions were as per Figure 6; image shown is representative of those seen from at least two such fields of view per sample and two independent samples; scale bar is 1 µm

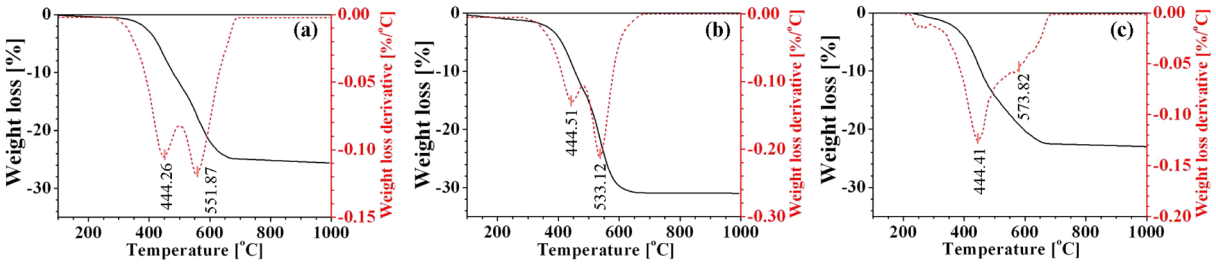


**Fig. 6** TG/DTG curves of the product synthesized at ethylene concentrations of (a) 37.5 mol%, (b) 50.0 mol% and (c) 62.5 mol%; reactions were performed with 20 g catalyst for 60 min at fixed $H_2$ flow of 200 sscm and varying the ethylene: $N_2$ flow from 300 : 300 to 500 : 100 sscm; curves shown are representative of those seen from two independent samples

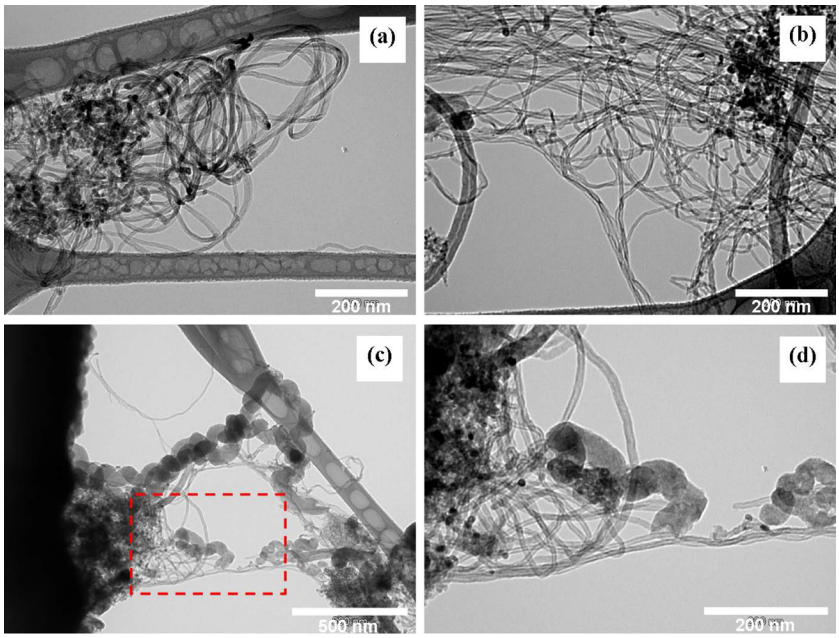


**Fig. 8** TEM images of the product synthesized at ethylene concentration of (a) 37.5 mol%, (b) 50.0 mol% and (c) 62.5 mol%, and (d) an enlargement of indicated area (red dashed oblong) in (c); other reaction conditions were as per Figure 6; images shown are representative of those seen from at least three such fields of view per sample and two independent samples; scale bars are 200 nm for (a), (b) and (d), and 500 nm for (c)

reduced the reproducibility of data, as seen from the wide spread of the data obtained at 37.5 mol% ethylene.

However, further increasing the ethylene concentration to 62.5 mol% resulted in a marked decrease in the solid carbon conversion level (3.2-fold lower, to a 1.1-fold lower level than that at 37.5 mol% ethylene) and the MWCNT selectivity (two-fold lower). Under this ethylene rich atmosphere, the dissociation of ethylene itself can take place at a faster rate than the formation of MWCNTs, leading to the formation of excessive carbon precursors (Escobar *et al.*, 2007). The excess precursors then become amorphous carbon, which nucleate more easily than MWCNTs, thereby resulting in the low MWCNT selectivity. Moreover, the amorphous carbon can cover the catalyst surface and hinder the reactant transport, thereby reducing the level of solid carbon conversion (Escobar *et al.*, 2007). SEM analysis of the product formed at a 62.5 mol% ethylene supported the presence of amorphous carbon (**Figure 7**), as do the TEM images of the MWCNTs (**Figure 8**).

### 2.3 Crystallinity of the synthesized MWCNTs

2.3.1 Influence of the synthesis temperature The XRD patterns of the products synthesized at different temperatures are shown in **Figure 9**. After MWCNTs synthesis, the metallic Co (in the form of $Co_3O_4$) peaks located at $2\theta = 19.0°$ (1 1 1), 31.3° (2 2 0), 36.8° (3 1 1) and 59.4° (5 1 1) disappeared, but the peaks of carbon (0 0 2) at $2\theta = \sim 26.5°$ and cobalt carbide ($Co_3C$) at $2\theta = 44.1°$ were still evident. Note that the diffraction peak located at 37.6° did not arise from (3 1 1) $Co_3O_4$, but was from (3 1 1) $\gamma$-$Al_2O_3$. The presence of $Co_3C$, concurrent with the absence of Co, indicates the formation of carbide, which has been reported to be an essential step for the growth of MWCNTs (Stamatin *et al.*, 2007; Sharma *et al.*, 2009; Wirth *et al.*, 2012; Pellegrino *et al.*, 2013).

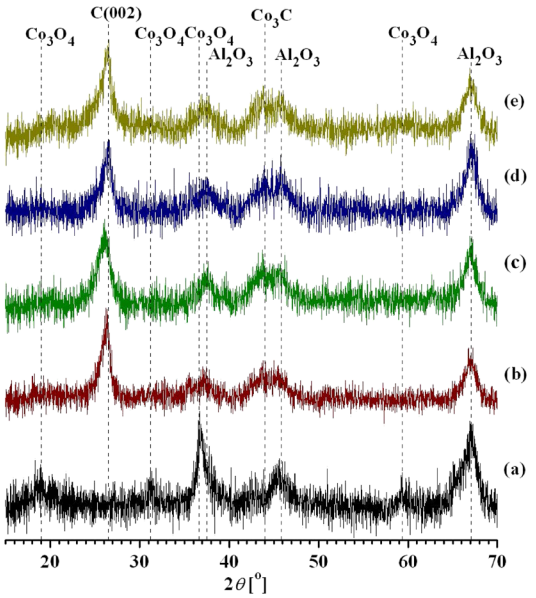


**Fig. 9** XRD patterns of the (a) fresh catalyst and the products synthesized at (b) 550°C, (c) 600°C, (d) 650°C and (e) 700°C; other reaction conditions are as in Figure 5; patterns shown are representative of those seen from two independent samples

According to Bragg's law, the carbon (0 0 2) diffraction peak can be used to determine the interplanar distance ($d$) (0 0 2) between the walls of the nanotubes. For graphitic carbon, the interplanar distance can be converted to the degree of graphitization ($g$) using the Maire and Mering formula (Maire and Mering, 1970), as shown in Eq. (3).

**Table 4** XRD analysis of the products synthesized at various temperatures

| Temperature [°C] | $2\theta_{max}$ [°] | $d$ (0 0 2) [Å] | Degree of graphitization [%] |
|---|---|---|---|
| 550 | 26.216 | 3.397 | 50.44 |
| 600 | 26.268 | 3.390 | 58.10 |
| 650 | 26.384 | 3.375 | 75.23 |
| 700 | 26.407 | 3.372 | 78.57 |

Data shown are representative of those seen from two independent samples.

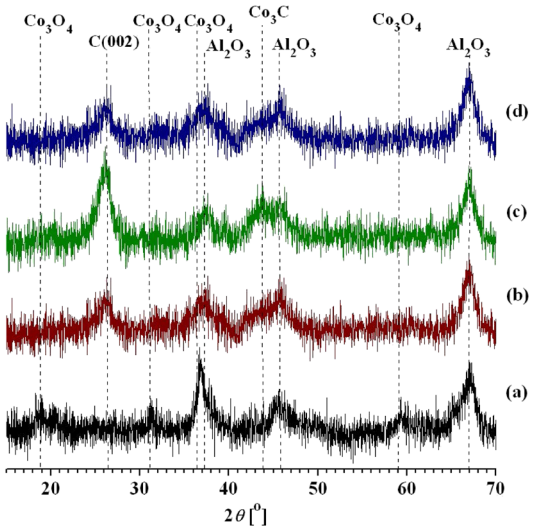


**Fig. 10** XRD patterns of the products synthesized at ethylene concentrations of (a) 0 mol%, (b) 37.5 mol%, (c) 50.0 mol% and (d) 62.5 mol%; other reaction conditions were as per Figure 6; patterns shown are representative of those seen from two independent samples

$$d(0\ 0\ 2) = 3.354 + 0.086(100 - g) \quad (3)$$

Herein, $d$ (0 0 2) is in angstroms and $g$ is in percent.

The effect of temperature on the crystallinity of the obtained MWCNTs, in terms of the degree of graphitization, is given in **Table 4**. The carbon (0 0 2) diffraction peak of the products increased slightly as the reaction temperature increased, which reflects the decreased (0 0 2) spacing. The degree of graphitization, calculated from the carbon (0 0 2) spacing, increased as the reaction temperature increased, being most marked at a temperature increase from 600 to 650°C (1.3-fold), while overall it increased 1.56-fold between 550 and 700°C. This confirmed that temperature plays a key role in the formation of well graphitized MWCNTs. Thus, it is noteworthy that the products synthesized at 550 and 600°C showed a moderate degree of graphitization, in agreement with their low oxidation temperatures ($T_o$) (Section 2.2.1), compared to those synthesized at 650 and 700°C. Potentially, the poor crystallinity of the MWCNTs (or CNFs) produced at these two temperatures resulted in the low thermal stability under an oxidizing atmosphere.

2.3.2 Influence of the ethylene concentration [mol%]

The XRD patterns of the products synthesized at various ethylene concentrations are shown in **Figure 10**, where the product synthesized at an ethylene concentration of 37.5 mol% showed a weak carbon (0 0 2) diffraction peak because of the low amount of MWCNTs (Section 2.2.2).

When the ethylene concentration was increased from 37.5 mol% to 50.0 mol%, an obvious carbon (0 0 2) diffraction peak was found at $2\theta = 26.268°$, indicating the presence of MWCNTs. On the other hand, further increasing the ethylene concentration to 62.5 mol% resulted in an ambiguous carbon (0 0 2) diffraction peak due to the presence of

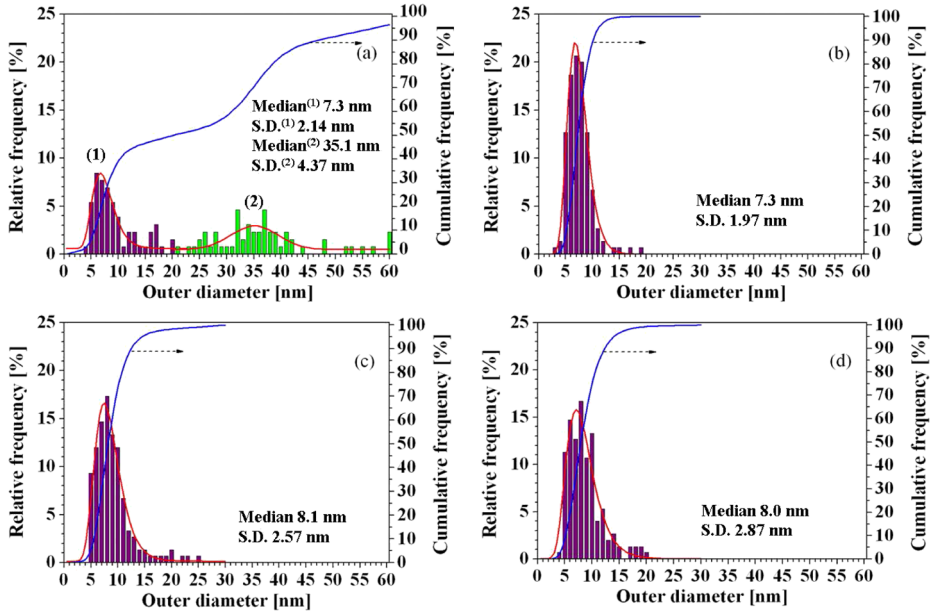


**Fig. 11** Size distribution (outer diameter) of the MWCNTs synthesized at (a) 550°C, (b) 600°C, (c) 650°C and (d) 700°C; other reaction conditions were as per Figure 5; data shown are representative of those seen from two independent samples

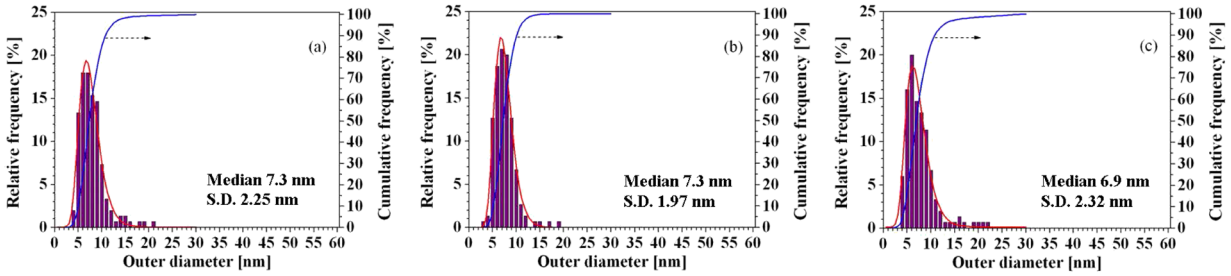


**Fig. 12** Size distribution (outer diameter) of the MWCNTs synthesized at ethylene concentrations of (a) 37.5 mol%, (b) 50.0 mol% and (c) 62.5 mol%; other reaction conditions were as per Figure 6; data shown are representative of those seen from two independent samples

amorphous carbon as the major product. For the products synthesized at ethylene concentrations of 37.5 and 62.5 mol%, the evaluation of the product crystallinity, in terms of the interplanar distance, and the degree of graphitization would likely be inaccurate and unreliable because of the indistinct carbon (0 0 2) diffraction.

### 2.4 Size distribution of the synthesized MWCNTs

The size distribution of the synthesized MWCNTs was determined from the TEM images. Manipulation of the raw TEM images (e.g., brightness/contrast adjustment and background subtraction) was performed using the ImageJ image processing program in order to facilitate observation of individual nanotube boundaries. For each sample, the outer diameters of 150 distinct tubes were measured and are shown along with the best-fit statistical model (**Figures 11** and **12**).

2.4.1 Influence of temperature on the synthesis of MWCNTs The outer diameter of the product synthesized at 550°C (Figure 11(a)) contained two distinct populations with different attributes. The first had a narrow size range of 4–12 nm and conformed to a log-normal distribution with an average (median) diameter of 7.3±2.14 nm, while the second population was larger and more broadly but normally distributed (20–60 nm), with an average (median) diameter of 35.1±4.37 nm.

The bimodal size distribution of the products synthesized at 550°C reflects the coexistence of the smaller MWCNTs and the larger CNFs. At higher growth temperatures (Figure 11(b)–(d)), no CNFs were detected and the average (median) outer diameter of the MWCNT populations synthesized at 600, 650 and 700°C were 7.3±1.97, 8.1±2.57 and 8.0±2.87 nm, respectively.

Note that the size distribution of the as-prepared MWCNTs fit well to a log-normal profile instead of a Gaussian (normal) distribution. This deviation from a Gaussian profile is due to the absence of any product with outer diameters smaller than 3 nm, which corresponds to the typical outer diameter of single-walled or double-walled CNTs.

2.4.2 Influence of the ethylene concentration [mol%] The size distribution of the MWCNTs synthesized at an ethylene concentration of 37.5, 50.0 and 62.5 mol% were all quite similar, and conformed to a log-normal distribution with an average (median) outer diameter of 7.3±2.25, 7.3±1.97 and 6.9±2.32 nm, respectively (**Figure 12**).

Thus, the reaction temperature and the ethylene molar percentage did not significantly affect the size distribution of MWCNTs. The average outer diameters of the synthesized MWCNTs were in the range of 7–8 nm, which is quite close to the crystallite size of $Co^0$. This is in accord with the notion that the outer diameter of MWCNTs is controlled by the size of the active metal (Sato *et al.*, 2003).

### 2.5 Kinetics of MWCNT synthesis, evaluated by online analysis

The growth of MWCNTs over time was evaluated by performing an overall carbon balance. The chemical composition of the effluent ($N_2$, $H_2$, methane, ethane, ethylene and/or other carbonaceous gases), was examined by GC, and was then converted to the equivalent mass of output carbon.

The mass of carbonaceous deposits (amorphous carbon+MWCNTs) was simply calculated by taking the difference between the mass of the input and output carbon. Multiplying the mass of carbonaceous deposits by the MWCNT selectivity (obtained from the TG/DTG analysis) yielded the mass of MWCNTs. Note that this evaluation was performed assuming a constant MWCNT selectivity at different reaction times, using the sample obtained at the end of experiment as representative. In addition, it was carried out by adding a three-fold higher amount of catalyst to ensure that there was enough metal available for the growth of MWCNTs, thereby minimizing amorphous carbon formation, especially at high temperatures where a rapid decomposition/dissociation of precursors takes place.

From the GC analysis, the effluent was found to be composed of $N_2$, $H_2$, ethane and methane without any unreacted ethylene being detected, indicating 100% ethylene conversion. The MWCNTs, and the other carbonaceous products mentioned above, could be generated via the reactions shown in Eqs. (4)–(6) (Philippe *et al.*, 2009).

$$C_2H_4 \rightarrow 2C + 2H_2 \quad (4)$$

$$C_2H_4 + H_2 \rightarrow C_2H_6 \quad (5)$$

$$C_2H_4 + 2H_2 \rightarrow 2CH_4 \quad (6)$$

At a reaction temperature of 700°C, a partial agglomeration of the bed was encountered during the last 10 min of the reaction, and thus the data collected during this period (50–60 min) were omitted from the analysis.

The distribution of carbon in the products with respect to the reaction temperature and time is shown in **Figure 13**.

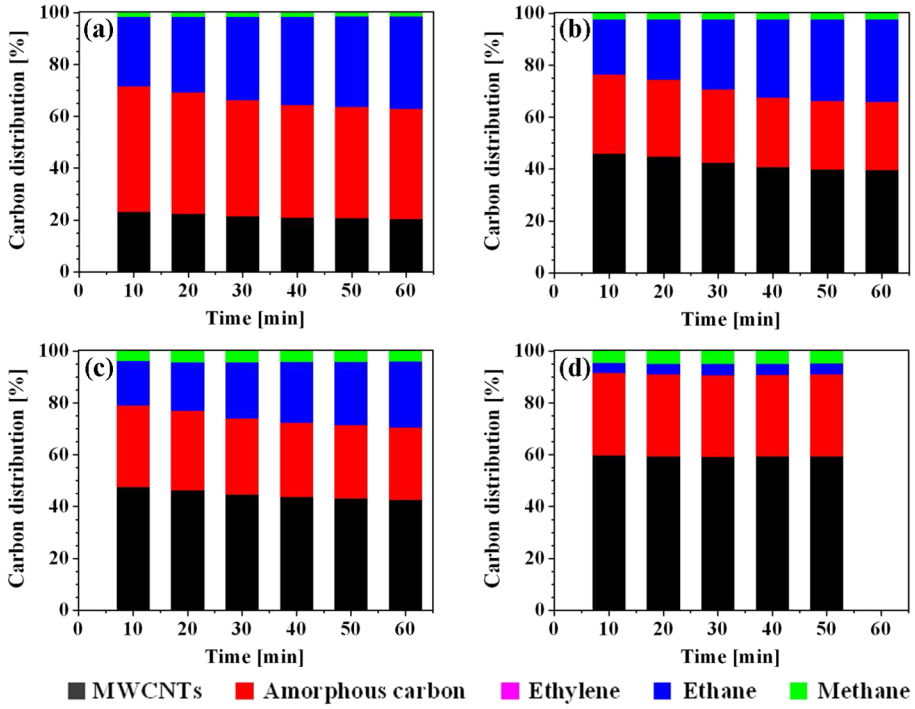


**Fig. 13** The distribution of carbon in the products with respect to time at (a) 600°C, (b) 650°C, (c) 675°C and (d) 700°C

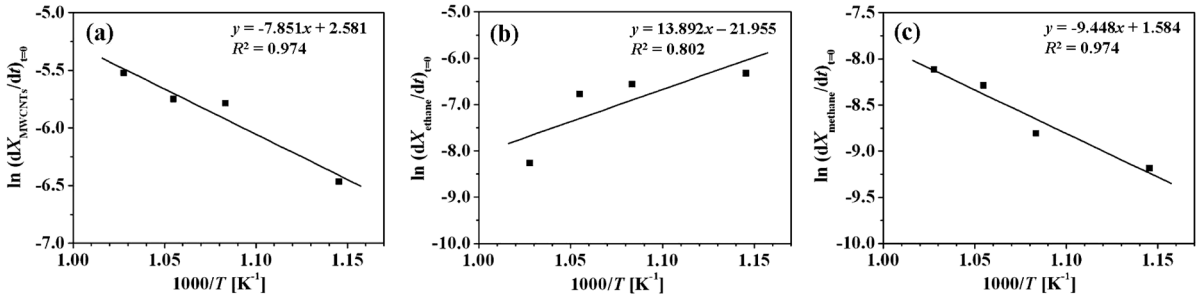


**Fig. 14** Arrhenius plots of the productivity of (a) MWCNTs, (b) ethane and (c) methane; the best fit linear regression line and its equation are shown for each plot, along with the linear regression correlation coefficient ($R^2$)

Over the temperature range studied (600–700°C), the level of MWCNT production (black bar) increased considerably with increasing reaction time and temperature, and was most marked between 600–650°C, and from 675–700°C.

The first marked increase, between 600 and 650°C, was derived from the 1.85-fold increase in the MWCNT selectivity (32.6 and 60.2% at 600 and 650°C, respectively), whilst the solid carbon conversion level was essentially constant (e.g., 63.7 and 66.3% at 600 and 650°C, respectively, after 50 min). The increased MWCNT selectivity with an essentially unchanged solid carbon conversion level indicates that 600°C is just sufficient to drive the dissociation of ethylene, but not for the formation of MWCNTs; whereas, 650°C is sufficient for both. Therefore, the product obtained at 600°C is mainly amorphous carbon, which grows more easily than MWCNTs, resulting in the relatively low MWCNT selectivity. On the other hand, the second marked increment of MWCNT production level, between 675 and 700°C, was mainly caused by the 1.27-fold increase in the solid carbon conversion level (e.g., 71.5 and 91.1% at 50 min for 675 and 700°C, respectively), while the MWCNT selectivity only slightly (<1.1-fold) increased (60.4 and 65.4% at 675 and 700°C, respectively). In addition, the ethane production level (blue bar), which tended to decrease with increasing reaction temperatures, was dramatically lower at 700°C than at lower temperatures (5.75- to 7.85-fold for 675 to 600°C, respectively). The substantial increase in the solid carbon conversion, concurrent with the sharp decrease in the level of ethane production at 700°C, indicates that the dehydrogenation of ethylene to form deposited carbon (Eq. (4)) was the most favored reaction; whereas, the hydrogenation of ethylene to form alkanes became much less pronounced at this temperature. In this study, the methane production level (green bar) continually increased with temperature, but nevertheless remained much lower than that of the MWCNTs and ethane, being almost negligible.

The kinetics of each reaction was investigated using the Arrhenius law (Eq. (7)).

$$\ln(dX/dt) = \ln(k_0) - E_a / RT \quad (7)$$

Herein, $dX/dt$ is the rate of productivity observed from the slope of productivity at the time of interest, $k_0$ is the apparent pre-exponential coefficient and $E_a$ is the apparent activation energy of the reaction. The kinetic parameters of the formation of MWCNTs, ethane and methane at the initial times ($t = 0$) were evaluated. From the plots of $\ln(dX/dt)$ versus the reciprocal of the reaction temperature in Kelvin, the activation energy of the reaction and the apparent pre-exponential coefficient were deduced from the slope and Y-intercept, respectively.

The Arrhenius plots for the formation of MWCNTs, ethane and methane production are illustrated in **Figure 14**. For the formation of MWCNTs, $E_a$ and $k_0$ were found to be 65.3 kJ/mol and 13.21 $g_C/g_{cat}$/min, respectively. For ethane production, because ethane productivity decreased over the temperature range studied, the Arrhenius plot gave a negative activation energy (so-called deactivation energy) of −115.5 kJ/mol, while $k_0$ was found to be $2.92\times10^{-10}$ $g_C/g_{cat}$/min. Due to the significant change in the selectivity of ethane production at 700°C, the data at this temperature deviated from a linear trend and, therefore, was of reduced reliability, as seen in Figure 14(b). Finally, for methane formation, $E_a$ and $k_0$ were 78.5 kJ/mol and 4.87 $g_C/g_{cat}$/min, respectively.

Concerning the rate determining step, different rate-determining steps for CVD growth of CNTs have previously been reported, including gas diffusion, dissociation of precursor and carbon diffusion. In this work, we believe that neither gas diffusion nor dissociation of the carbon precursor is the rate-determining step because of the following observations.

1. Gas diffusion as a rate-determining step has mainly been reported with densely aligned CNT forests because they can hinder the diffusion of the carbon precursor to the catalyst.
2. Ethylene has been reported to be completely dehydrogenated /dissociated to surface atomic carbon over Co at temperatures above 223°C (Tiscione and Rovida, 1985; Xu *et al.*, 2012a). At higher temperatures, the rapid dissociation of ethylene would likely be attained.
3. The activation energy for the dissociation of absorbed carbon species into atomic carbon on various metal catalysts was predicted using density functional theory to be in the range of 140–150 kJ/mol for Ni (Hofmann *et al.*, 2005; Basarana *et al.*, 2011) and ~100 kJ/mol for Fe (Lee *et al.*, 2002). Since cobalt usually shows an intermediate reactivity between Fe and Ni (Tiscione and Rovida, 1985), it is expected to have an $E_a$ in the 100–150 kJ/mol range, which is inconsistent with our finding.

We, therefore, focused on the carbon diffusion as the rate determining step. Based on the vapor–solid–solid model (Ramírez *et al.*, 1999; Pirard *et al.*, 2007; Philippe *et al.*, 2009), the activation energy of MWCNTs growing on a Co catalyst was previously reported to be close to that of carbon diffusion into solid metal, at ~150 kJ/mol, which is still inconsistent with the value obtained in this work.

However, for the vapor–liquid–solid model (Bartsch and Leonhardt, 2004; Zhukov *et al.*, 2010), the activation energy of carbon diffusion into liquid Co was reported to be ~59 kJ/mol (Zhukov *et* al., 2010). Considering the level of uncertainty of the kinetic parameter estimation, the difference between the $E_a$ obtained in this work and the value reported by Zhukov is somewhat acceptable. It is, therefore, possible that carbon diffusion into liquid Co is the rate determining step. This idea is supported by the observation that the melting temperature of Co nanoparticles with an average size of 30 nm was reported to start from 600°C under a carburizing atmosphere or from 650°C under an inert atmosphere (Homma *et al.*, 2003). The dramatic decrease in the melting temperature of metal nanoparticles is because of their high surface to volume ratio and the formation of eutectic carbides (Homma *et al.*, 2003; Moisala *et al.*, 2003).

## Conclusion

MWCNTs were successfully synthesized in a fluidized-bed reactor using $Co/Al_2O_3$ as the catalyst. The reaction temperature and the ethylene (carbon precursor) concentration were crucial parameters for the production of MWCNTs. A change in reaction temperature resulted in a significant change in the type of the product, MWCNTs productivity as well as graphitic crystallinity. A reaction temperature of 550°C gave a low solid carbon drive the conversion level due to providing insufficient external energy to ethylene dissociation. Moreover, the selectivity of MWCNT formation was low due to the presence of CNFs as co-products. The formation of MWCNTs showed a positive order dependence on the ethylene concentration, but increasing the ethylene concentration above 50 mol% led to catalyst poisoning. However, both reaction temperature and ethylene concentration did not influence the size distribution of MWCNTs.

The dehydrogenation of ethylene to form MWCNTs occurred preferentially at temperatures above 675°C. The apparent activation energy for MWCNTs synthesis was found to be 65.3 kJ/mol, which is in accordance with that for the diffusion of carbon into liquid cobalt. Considering both the quality and quantity aspects, the suitable temperature for synthesis of MWCNTs via FB-CCVD was 650°C, which yielded MWCNTs with a 75% degree of graphitization at 7.3 g/g of metallic Co.

#### Acknowledgements

The authors gratefully acknowledge the financial support of the Thailand Research Fund and the embassy of France in Thailand through the Royal Golden Jubilee Ph.D. Program to Sompoch Pooperasupong and Somsak Damronglerd (Grant No. PHD/0125/2547). We are grateful to Arkema Inc., scientists and technicians at ENSIACET/INPT and Chulalongkorn University, especially to Michel Molinier, for their support and helpful assistance. We also thank the anonymous reviewers whose comments improved this manuscript, and Dr. Robert Douglas

John Butcher for his help in editing the manuscript under the service of the Publication Counseling Unit of the Faculty of Science, Chulalongkorn University.

## Nomenclature

| | | | |
|---|---|---|---|
| $a$ | = | kinetic order | [−] |
| $d$ (0 0 2) | = | carbon (0 0 2) interplanar distance | [Å] |
| $D_{[4,3]}$ | = | volume weighted mean diameter of particle | [μm] |
| $D_{Co^0}$ | = | mean crystallite size of $Co^0$ | [nm] |
| $D_{Co_3O_4}$ | = | mean crystallite size of $Co_3O_4$ | [nm] |
| $E_a$ | = | apparent activation energy of reaction | [kJ/mol] |
| $g$ | = | degree of graphitization | [%] |
| $k_0$ | = | apparent pre-exponential coefficient | [−] |
| $T_o$ | = | temperature at the maximum in the weight loss rate | [°C] |
| $U$ | = | superficial velocity | [cm/s] |
| $U_{mf}$ | = | minimum fluidization velocity | [cm/s] |
| $X$ | = | productivity | [$g_C/g_{cata}$] |
| | | | |
| $\rho_b$ | = | untapped bulk density | [g/cm] |
| $\rho_g$ | = | grain density | [g/cm] |

## Literature Cited


Baddour, C. E., F. Fadlallah, D. Nasuhoglu, R. Mitra, L. Vandsburger and J. L. Meunier; "A Simple Thermal CVD Method for Carbon Nanotube Synthesis on Stainless Steel 304 without the Addition of an External Catalyst," *Carbon*, **47**, 313–318 (2009)

Bartsch, K. and A. Leonhardt; "Growth and Morphology of Aligned Carbon Nanotube Layers," *Thin Solid Films*, **469–470**, 115–119 (2004)

Basarana, D., H. A. Aleksandrov, Z.-X. Chen, Z.-J. Zhao and N. Rösch; "Decomposition of Ethylene on Transition Metal Surfaces M (1 1 1). A Comparative DFT Study of Model Reactions for M = Pd, Pt, Rh, Ni," *J. Mol. Catal. Chem.*, **344**, 37–46 (2011)

Camilli, L., M. Scarselli, S. Del Gobbo, P. Castrucci, F. Nanni, E. Gautron, S. Lefrant and M. De Crescenzi; "The Synthesis and Characterization of Carbon Nanotubes Grown by Chemical Vapor Deposition Using a Stainless Steel Catalyst," *Carbon*, **49**, 3307–3315 (2011)

Corrias, M., Y. Kihn, P. Kalck and P. Serp; "CVD from Ethylene on Cobalt Ferrite Catalysts: The Effect of the Support," *Carbon*, **43**, 2820–2823 (2005)

Danafar, F., A. Fakhru'l-Razi, M. A. M. Salleh and D. R. A. Biak; "Fluidized Bed Catalytic Chemical Vapor Deposition Synthesis of Carbon Nanotubes—A Review," *Chem. Eng. J.*, **155**, 37–48 (2009)

Escobar, M., M. S. Moreno, R. J. Candal, M. C. Marchi, A. Caso, P. I. Polosecki, H. G. Rubiolo and S. Goyanes; "Synthesis of Carbon Nanotubes by CVD: Effect of Acetylene Pressure on Nanotubes Characteristics," *Appl. Surf. Sci.*, **254**, 251–256 (2007)

Gulino, G., R. Vieira, J. Amadou, P. Nguyen, M. J. Ledoux, S. Galvagno, G. Centi and C. Pham-Huu; "$C_2H_6$ as an Active Carbon Source for a Large Scale Synthesis of Carbon Nanotubes by Chemical Vapour Deposition," *Appl. Catal. A*, **279**, 89–97 (2005)

Hofmann, S., G. Csányi, A. C. Ferrari, M. C. Payne and J. Robertson; "Surface Diffusion: The Low Activation Energy Path for Nanotube Growth," *Phys. Rev. Lett.*, **95**, 036101 (2005)

Homma, Y., Y. Kobayashi, T. Ogino, D. Takagi, R. Ito, Y. J. Jung and P. M. Ajayan; "Role of Transition Metal Catalysts in Single-Walled Carbon Nanotube Growth in Chemical Vapor Deposition," *J. Phys. Chem. B*, **107**, 12161–12164 (2003)

Huang, S., Q. Cai, J. Chen, Y. Qian and L. Zhang; "Metal-Catalyst-Free Growth of Single-Walled Carbon Nanotubes on Substrates," *J. Am. Chem. Soc.*, **131**, 2094–2095 (2009)

Iijima, S.; "Helical Microtubules of Graphitic Carbon," *Nature*, **354**, 56–58 (1991)

Kumar, M. and Y. Ando; "Chemical Vapor Deposition of Carbon Nanotubes: A Review on Growth Mechanism and Mass Production," *J. Nanosci. Nanotechnol.*, **10**, 3739–3758 (2010)

Lee, G. D., S. Han, J. Yu and J. Ihm; "Catalytic Decomposition of Acetylene on Fe(001): A First-principles Study," *Phys. Rev. B*, **66**, 081403(R) (2002)

Maire, J. and J. Mering; "Graphitization of Soft Carbons," Chemical and Physics of Carbon, vol. 6, pp. 125–190, Marcel Dekker, New York, U.S.A. (1970)

McCaldin, S., M. Bououdina, D. M. Grant and G. S. Walker; "The Effect of Processing Conditions on Carbon Nanostructures Formed on an Iron-Based Catalyst," *Carbon*, **44**, 2273–2280 (2006)

Moisala, A., A. G. Nasibulin and E. I. Kauppinen; "The Role of Metal Nanoparticles in the Catalytic Production of Single-Walled Carbon Nanotubes—A Review," *J. Phys. Condens. Matter*, **15**, S3011–S3035 (2003)

Morançais, A., B. Caussat, Y. Kihn, P. Kalck, D. Plee, P. Gaillard, D. Bernard and P. Serp; "A Parametric Study of the Large Scale Production of Multi-Walled Carbon Nanotubes by Fluidized Bed Catalytic Chemical Vapor Deposition," *Carbon*, **45**, 624–635 (2007)

Paradise, M. and T. Goswami; "Carbon Nanotubes—Production and Industrial Applications," *Mater. Des.*, **28**, 1477–1489 (2007)

Pellegrino, L., M. Daghetta, R. Pelosato, A. Citterio and C. V. Mazzocchia; "Searching for Rate Determining Step of CNT Formation: The Role of Cementite," *Chem. Eng. Trans.*, **32**, 739–744 (2013)

Philippe, R., A. Morançais, M. Corrias, B. Caussat, Y. Kihn, P. Kalck, D. Plee, P. Gaillard, D. Bernard and P. Serp; "Catalytic Production of Carbon Nanotubes by Fluidized-Bed CVD," *Chem. Vapor Depos*, **13**, 447–457 (2007)

Philippe, R., P. Serp, P. Kalck, Y. Kihn, S. Bordère, D. Plee, P. Gaillard, D. Bernard and B. Caussat; "Kinetic Study of Carbon Nanotubes Synthesis by Fluidized Bed Chemical Vapor Deposition," *AIChE J.*, **55**, 450–464 (2009)

Pirard, S. L., S. Douven, C. Bossuot, G. Heyen and J. P. Pirard; "A Kinetic Study of Multi-Walled Carbon Nanotube Synthesis by Catalytic Chemical Vapor Deposition Using a Fe–Co/$Al_2O_3$ Catalyst," *Carbon*, **45**, 1167–1175 (2007)

Ramírez, A. G., T. Itoh and R. Sinclair; "Crystallization of Amorphous Carbon Thin Films in the Presence of Magnetic Media," *J. Appl. Phys.*, **85**, 1508–1513 (1999)

Sato, S., A. Kawabata, M. Nihei and Y. Awano; "Growth of Diameter-Controlled Carbon Nanotubes Using Monodisperse Nickel Nanoparticles Obtained with a Differential Mobility Analyzer," *Chem. Phys. Lett.*, **382**, 361–366 (2003)

Schanke, D., S. Vada, E. A. Blekkan, A. M. Hilmen, A. Hoff and A. Holmen; "Study of Pt-Promoted Cobalt CO Hydrogenation Catalysts," *J. Catal.*, **156**, 85–95 (1995)

See, C. H. and A. T. Harris; "A Review of Carbon Nanotube Synthesis via Fluidized-Bed Chemical Vapor Deposition," *Ind. Eng. Chem. Res.*, **46**, 997–1012 (2007)

Serp, P., M. Corrias and P. Kalck; "Carbon Nanotubes and Nanofibers in Catalysis," *Appl. Catal. A*, **253**, 337–358 (2003)

Sharma, R., E. Moore, P. Rez and M. M. J. Treacy; "Site-Specific Fabrication of Fe Particles for Carbon Nanotube Growth," *Nano Lett.*, **9**, 689–694 (2009)

Somanathan, T. and A. Pandurangan; "Towards the Low Temperature Growth of Uniform Diameter Multi Walled Carbon Nanotubes by Catalytic Chemical Vapour Deposition Technique," *Nano-Micro*

*Lett.*, **2**, 204–212 (2010)

Stamatin, I., A. Morozan, A. Dumitru, V. Ciupina, G. Prodan, J. Niewolski and H. Figiel; "The Synthesis of Multi-Walled Carbon Nanotubes (MWCNTs) by Catalytic Pyrolysis of the Phenol–Formaldehyde Resins," *Physica E*, **37**, 44–48 (2007)

Terrones, M.; "Science and Technology of the Twenty-First Century: Synthesis, Properties, and Applications of Carbon Nanotubes," *Annu. Rev. Mater. Res.*, **33**, 419–501 (2003)

Tiscione, P. and D. Rovida; "Adsorption and Decomposition of Ethylene and Acetylene on Cobalt," *Surf. Sci.*, **154**, L255–L260 (1985)

Vahlas, C., B. Caussat, P. Serp and G. N. Angelopoulos; "Principles and Applications of CVD Powder Technology," *Mater. Sci. Eng. Rep.*, **53**, 1–72 (2006)

Venegoni, D., P. Serp, R. Feurer, Y. Kihn, C. Vahlas and P. Kalck; "Parametric Study for the Growth of Carbon Nanotubes by Catalytic Chemical Vapor Deposition in a Fluidized Bed Reactor," *Carbon*, **40**, 1799–1807 (2002)

Wang, Y., F. Wei, G. Luo, H. Yu and G. Gu; "The Large-Scale Production of Carbon Nanotubes in a Nano-Agglomerate Fluidized-Bed Reactor," *Chem. Phys. Lett.*, **364**, 568–572 (2002)

Wirth, C. T., B. C. Bayer, A. D. Gamalski, S. Esconjauregui, R. S. Weatherup, C. Ducati, C. Baehtz, J. Robertson and S. Hofmann; "The Phase of Iron Catalyst Nanoparticles during Carbon Nanotube Growth," *Chem. Mater.*, **24**, 4633–4640 (2012)

Xu, L., Y. Ma, Z. Wu, B. Chen, Q. Yuan and W. Huang; "A Photoemission Study of Ethylene Decomposition on a Co(0001) Surface: Formation of Different Types of Carbon Species," *J. Phys. Chem. C*, **116**, 4167–4174 (2012a)

Xu, X., S. Huang, Y. Hu, J. Lu and Z. Yang; "Continuous Synthesis of Carbon Nanotubes Using a Metal-Free Catalyst by CVD," *Mater. Chem. Phys.*, **133**, 95–102 (2012b)

Zhang, Q., J. Q. Huang, M. Q. Zhao, W. Z. Qian and F. Wei; "Carbon Nanotube Mass Production: Principles and Processes," *ChemSusChem*, **4**, 864–889 (2011)

Zhukov, V. P., V. A. Kniss, S. V. Kniss and A. S. Avdeev; "Investigation of the Kinetics of Cobalt Decarburization in a Direct-Current Arc Furnace," *Russ. J. Non-Ferrous Met.*, **51**, 97–100 (2010)